Chemical Engineering Journal 529 (2026) 172570

Contents lists available at ScienceDirect

Chemical Engineering Journal

journal homepage: www.elsevier.com/locate/cej

Anode interface layers constructed *in situ* by multifunctional carbon dots for ultra-stable aqueous zinc-ion batteries

Qian-Li Ma, Xi-Rong Zhang, Bao-Juan Wang, Hao-Wen Sun, Huan-Ming Xiong *

Department of Chemistry, Shanghai Key Laboratory of Electrochemical and Thermochemical Conversion for Resources Recycling, Fudan University, Shanghai, 200438, PR China

ARTICLE INFO

Keywords:
Carbon dot
Aqueous zinc-ion battery
Electrolyte additive
Anode interface
pH buffer

ABSTRACT

Aqueous zinc-ion batteries (AZIBs), owing to their safety and low cost, are one of the most promising energy storage systems. But the uncontrollable dendrite growth and side reactions limit their practical application. Using electrolyte additives is a simple and effective method to optimize the battery performance. This paper presents a strategy of using carbon dots (CDs) to construct electrode protective layer *in situ*. A new kind of nitrogen and sulfur co-doped carbon dots (NSCDs) was designed for this aim, which help AZIBs achieve excellent performance by trace amounts (0.2 mg mL^{-1}) of addition. The interfacial protective layer formed by the adsorption of NSCDs on the Zn electrode surface enhances the stability of the electrode during deposition/stripping processes through the improved ion transport kinetics and the effective buffering of interfacial pH values. As a result, the Zn||Zn symmetric cell achieves a stable cycle of more than 4000 h, and the Zn||$NH_4V_4O_{10}$ full cell shows excellent specific capacity and capacity retention under a rapid charge/discharge condition of 3 A g^{-1}.

1. Introduction

In the past decade, aqueous zinc-ion batteries (AZIBs) have attracted intensive attention due to the abundant reserves of Zn, the safety of aqueous electrolytes, the high volumetric energy density (5855 mAh cm^{-3}), and the low reduction potential (0.762 V *vs.* standard hydrogen electrode) [1–4]. Among the numerous reports on AZIBs research, the greatest challenge arises from the instability of the zinc anode, involving the dendrite growth, the hydrogen evolution reaction (HER) and the by-product accumulation, which heavily reduce the cycle life and Coulomb efficiency of AZIBs [5]. To overcome the above problems, various methods have been tried, such as electrode surface coating [6], electrolyte modification [7,8], anode structure design [9], controlled growth of specific crystal faces [10], *etc.* It is adopted that introducing electrolyte additives is the simplest and most effective method [11,12]. Many electrolyte additives have been developed recently, which can be divided into two major categories: ionic additives (like Na^+ [13], Mg^{2+} [14], Pb^{2+} [15], Co^{2+} [16], *etc.*) and organic additives (like ethanol [17], PEG [18], tartaric acid [19], urea [20], *etc.*). Ionic additives are able to inhibit the dendrite growth by regulating the interfacial electric field, homogenizing the deposition kinetics, and promoting the homogeneous nucleation. Organic additives can adjust the Zn^{2+} solvation structure or the anode reaction kinetics through binding to zinc, so the corrosion and the dendrite growth on Zn anodes are suppressed. In addition, some organic additives can form hydrogen bonding network with water to hinder HER and improve the decomposition voltage of the aqueous electrolyte. Both HER and H^+/Zn^{2+} co-embedding phenomena are universal in AZIBs, which cause the pH value increase in the electrolytes and produce by-products. Some organic molecules possess both acidic groups and basic groups, and thus play as pH buffers to prevent the side reactions. Although there are plenty of additives for AZIBs in literature, it is difficult to find one that meets all requirements for stabilizing AZIBs.

Carbon dots (CDs) are a new family of organic-inorganic hybrid nanomaterials with excellent photoluminescence [21], whose electrochemical properties have been discovered recently and developed in many energy storage devices [22–25]. Among various nanoparticles applied in batteries, CDs have special advantages naturally. Their composition and structure can be easily adjusted to meet various requirements in batteries, their small size (1–10 nm) and rich surface groups allows their homogeneous dispersion in all kinds of electrolytes, and their nontoxicity, environmental friendship and sustainability match with the development of renewable energy [26–28]. Distinguished from those ionic additives and organic additives, CDs are

* Corresponding author.
E-mail address: hmxiong@fudan.edu.cn (H.-M. Xiong).

https://doi.org/10.1016/j.cej.2026.172570
Received 3 November 2025; Received in revised form 26 December 2025; Accepted 1 January 2026
Available online 6 January 2026

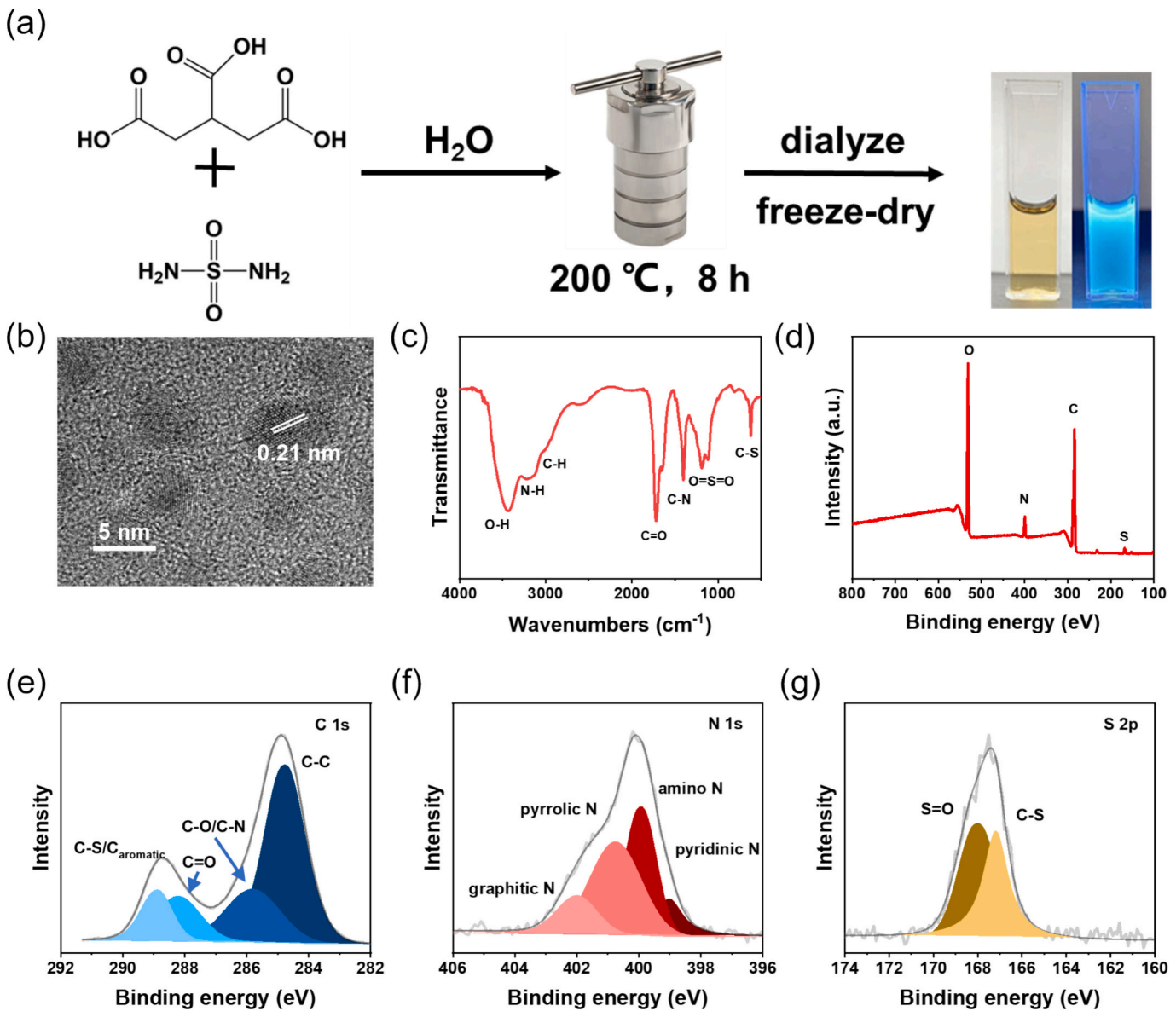

Fig. 1. (a) The method of NSCDs synthesis and NSCDs solution in sunlight and ultraviolet light; characterization of as-prepared NSCDs. (b) TEM image of NSCDs. (c) FTIR spectra of NSCDs. (d) The XPS full survey of NSCDs and deconvoluted high- resolution XPS of (e) C 1 s, (f) N 1 s, and (g) S 2p spectra of NSCDs, respectively.

nanoparticles with carbon cores and various surface groups, which means CDs will show multi-functions as a new type of additives in AZIBs.

Graphene quantum dots (GQDs) are one kind of CDs, which was first added in the electrolyte to suppress the reactivity of water and stabilize Zn anode successfully [29]. Another kind of CDs, C_3N_4 QDs was also employed to stabilize Zn anode through constructing a self-repairing interphase, where the periodic graphitic N sites guided the uniform deposition of zinc ions [30]. Subsequent researchers found that the doped CDs have more defects and active sites, and thus are more effective as AZIBs additives [31]. For example, our research group synthesized N, S-codoped CDs with rich polar surface groups, which could reduce anode corrosion by adjusting the solvation structure of zinc ions, and accelerate Zn^{2+} transfer from the electrolyte to Zn surface by the sulfonic groups on CDs surfaces [32]. Later, we found a kind of S-doped CDs could induce the formation of dense (002) crystal planes during the Zn deposition, further enhancing the stability of Zn anode for AZIBs [33]. Furthermore, carbonized polymer dots, as a subset of carbon dots, can also be used as electrolyte additives [34]. These functionalized CDs primarily focus on regulating Zn^{2+} transport behaviors at the electrode interfaces, yet overlook the detrimental effects of pH change induced by HER and H^+ insertion/extraction. The pH elevation of the electrolyte will produce irreversible byproducts, accelerate electrode passivation and ultimately compromise the cycling stability of AZIBs. It is necessary to find some multi-functional CDs to control zinc deposition homogenously and stabilize the pH values of the electrolyte simultaneously.

In this work, we synthesized a new kind of nitrogen-sulfur co-doped carbon dots (NSCDs) as multifunctional additives to construct an interfacial protective layer on Zn anode *in situ*. Through the modular molecular design, the NSCDs possess strong affinity to Zn electrodes and selective binding capability to Zn^{2+} ions. Trace amounts of NSCDs additives can effectively adhere onto the Zn electrode surface, and in the meantime, regulate the distribution and chemical environment of both Zn^{2+} ions and H_2O molecules within the Helmholtz layer, thereby suppressing Zn dendrite growth and the electrode corrosion synergistically. Furthermore, the NSCDs serve as efficient pH buffers to stabilize the interfacial pH fluctuations and mitigate the byproduct accumulation on the electrode surface. A trace amount of NSCDs (0.2 mg mL^{-1}) in the

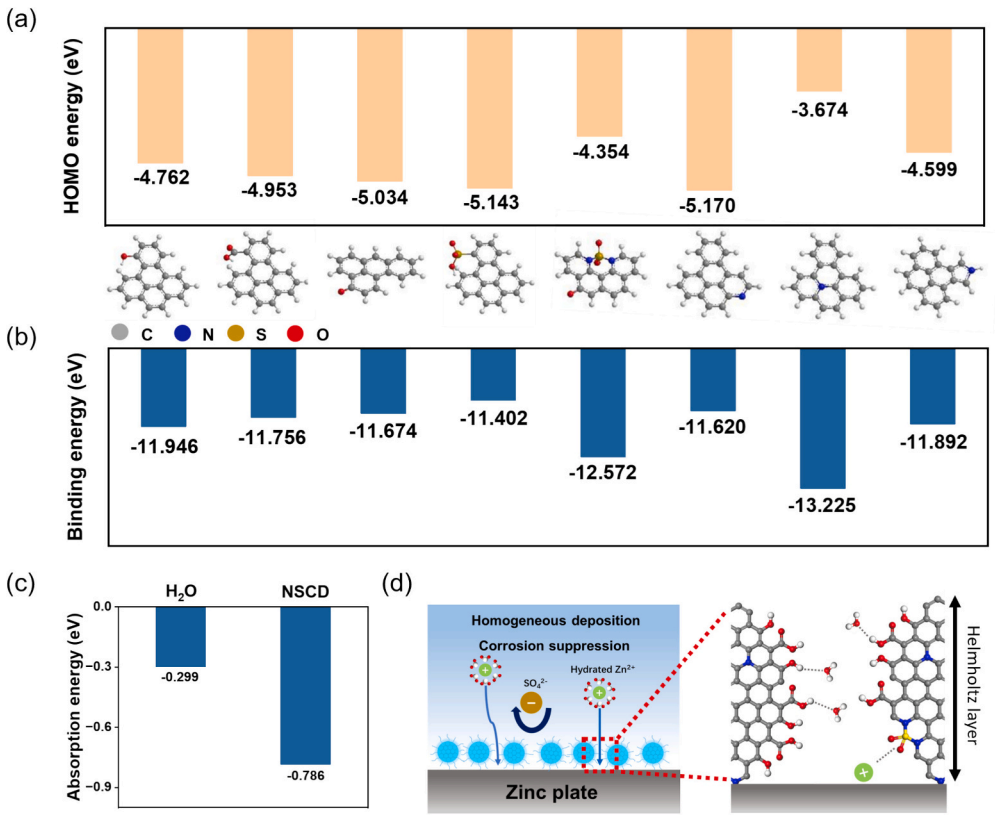

Fig. 2. Screening of functional groups and the influence of carbon dots on the zinc surface. (a) HOMO energy of carbon dots structure with different functional groups. (b) Binding energy between the zinc ion and different functional groups. (c) Adsorption energy of H_2O, NSCD on Zn (002) plane. (d)Schematic illustrations of the zinc plate in ZS-NSCD electrolyte.

typical 2 M $ZnSO_4$ electrolyte can significantly enhance the battery cycling stability. The Zn||Zn symmetric cells demonstrated exceptional cyclability, maintaining the stable operation for over 4000 h at a current density of 1 mA cm^{-2} and a capacity density of 0.5 mAh cm^{-2}. After the prolonged plating/stripping, the cells exhibited the remarkable interfacial stability and the dendrite-free morphology. When the above NSCDs incorporated electrolyte was tested in the Zn||$NH_4V_4O_{10}$ full cells, the cells could work stably for more than 1000 cycles under the current density of 3 A g^{-1} ($NH_4V_4O_{10}$ in coin cells).

2. Results and discussion

Experimentally, N and S co-doped CD (NSCDs) were synthesized by a simple hydrothermal reaction using citric acid and sulfonamide and then purified by dialysis, which resulted in aqueous solution with bright blue fluorescence under UV light (Fig. 1a). The transmission electron microscopy (TEM) image shows that such NSCDs are uniformly dispersed with an average diameter of about 7 nm (Fig. 1b). Their lattice structures are obvious with the interplanar spacing of 0.21 nm, corresponding to the (100) crystal plane of graphite [35]. NSCDs exhibit a low zeta potential of −18.6 mV (Fig. S1), indicating that their negatively charged surfaces are conducive to adsorb Zn^{2+} ions. FTIR measurement was performed to study the surface groups of NSCDs, and the obtained spectra (Fig. 1c) exhibit peaks at 1190 cm^{-1} and 621 cm^{-1} corresponding to the stretching vibrations of O=S=O and C—S, respectively [36,37]. The strong absorption FTIR peaks at 1720 and 1400 cm^{-1} are ascribed to C=O and C—N, respectively, indicating that NSCDs have plenty of amide structures. In addition, the peak at 1652 cm^{-1} corresponds to the C=C bonds, while the broad absorption band at 3600–3000 cm^{-1} is the typical signal of the electronegative -OH, -COOH, and -NH_2 groups [38–40]. X-ray photoelectron spectroscopy (XPS) was used to study the surface structures of NSCDs (Fig. 2d), and both N and S element peaks are observed in the full spectrum. In the high-resolution spectrum, the C 1 s spectrum can be divided into C—C, C-O/C-N, C=O, and C-S/$C_{aromatic}$ (Fig. 1e) [41], while the N1s spectrum can be fitted into pyrrole N, amino N, pyridine N, and graphite N, respectively (Fig. 1f) [42]. Moreover, the S 2p spectrum have two peaks at 166.4 eV and 168.1 eV, corresponding to C—S and S=O, respectively (Fig. 1g) [43]. The above characterization results prove that our NSCDs are doped with N and S successfully, with negatively charged surfaces and rich functional groups that will exhibit strong interactions with Zn.

The conduction band of zinc metal partially overlaps with the valence band, and the electrons in the valence band can easily transfer to the conduction band, thus forming unoccupied states in the valence band [44]. When the unoccupied states accept electrons from molecules or groups, chemical adsorption occurs on the surface of Zn. Structures with the higher HOMO (highest occupied molecular orbital) energy possess the stronger electron-donating capabilities, therefore, the HOMO energies of carbon dot structures are evaluated through the density functional theory (DFT) calculation, including amino N, graphite N, pyrrole N, pyridine N, carboxyl, carbonyl, sulfonamide group, and sulfonic group (Fig. 2a). Among them, the graphite N structure exhibits the highest HOMO energy (−5.170 eV), suggesting that NSCDs prefer to adsorb on the zinc metal surface through the graphite N structure. The binding energies of the above-mentioned structures with Zn^{2+} are calculated to assess the ability of NSCDs to guide the uniform deposition of Zn^{2+}. The results (Fig. 2b) indicate that both the graphite N and sulfonamide sites in NSCDs have good affinity for Zn^{2+}, and the carboxyl, hydroxyl, and amino groups on the surface of NSCDs also have relatively strong binding energies, much stronger than that of H_2O (−3.837 eV), which demonstrates that NSCDs can effectively regulate the solvation structure of Zn^{2+}. Subsequently, the adsorption behavior of NSCDs on the (002) crystal plane of zinc metal is evaluated by calculations, and the results (Fig. 2c) show that when NSCDs adsorb

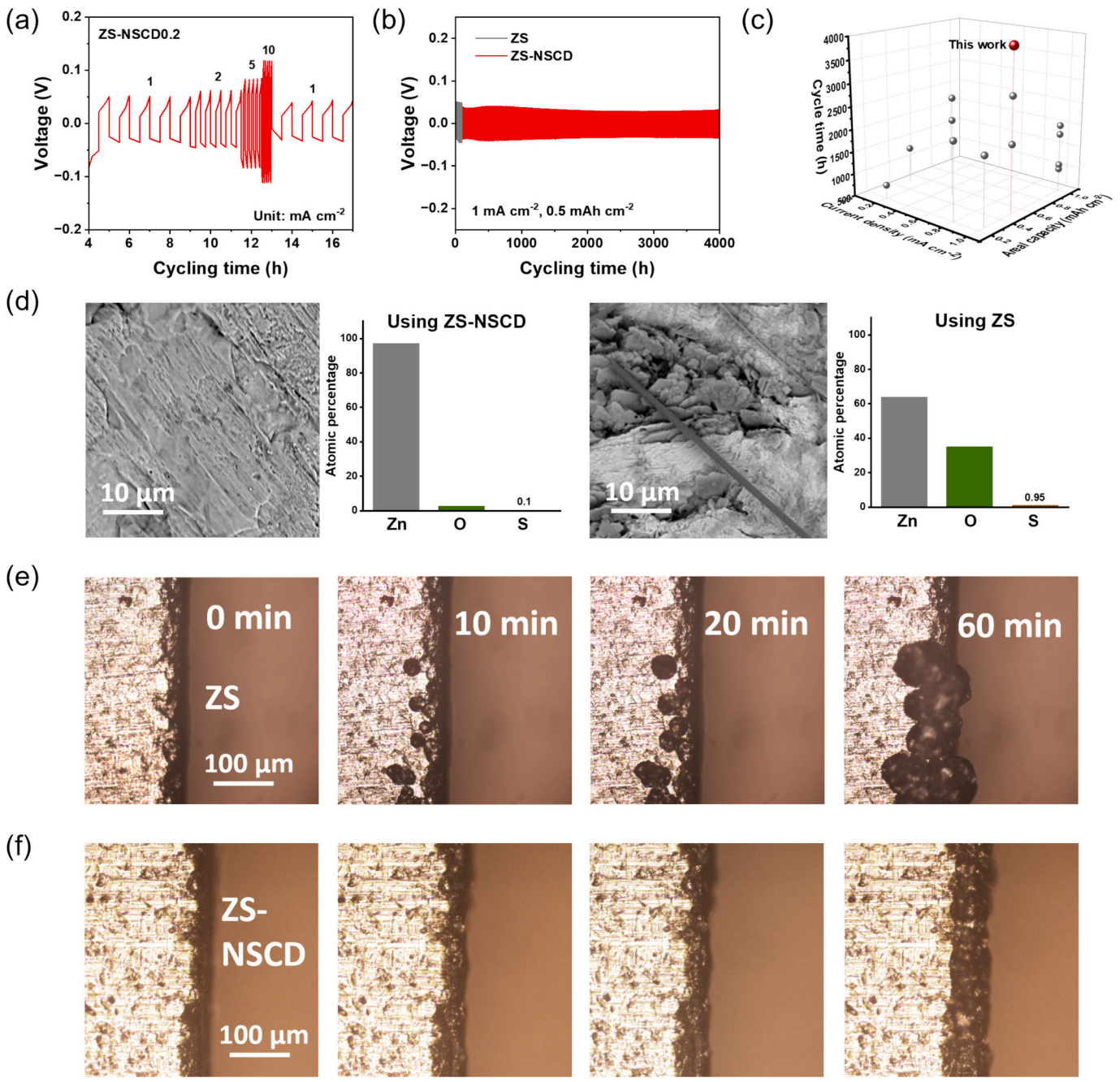

Fig. 3. (a) Rate performance of Zn||Zn cells in ZS-NSCD0.2 electrolyte. (b) Long-term galvanostatic charging/discharging of Zn||ZS-NSCD0.2||Zn cells under current density and areal capacity of 1 mA cm^{-2},0.5 mAh cm^{-2}. (c) Comparison of cycle time between this work and the literature. (d) SEM image and EDS analyzing of Zn plate after 50 cycles in Zn-NSCD0.2 electrolyte. (e)(f) *In-situ* optical microscopy images of Zn anode during Zn plating in ZS and ZS-NSCD0.2 electrolyte.

on the (002) crystal plane through the graphite N sites, the adsorption energy reaches −0.786 eV, which is much higher than the adsorption energy of H_2O molecules (−0.299 eV). This indicates that NSCDs can adsorb on the zinc metal surface preferentially compared to water molecules, thereby reducing the corrosion of the electrode by the active water [45]. Based on these findings, we propose a strategy to reconstruct the electrical double layer at the zinc electrode interface by NSCDs. The strong adsorption capability of graphitic nitrogen sites towards zinc metal enables NSCDs to replace water molecules in the Helmholtz layer, forming a new NSCD-dominated interfacial structure. Through the preferential coordination with Zn^{2+}, NSCDs effectively modify the Zn^{2+} solvation structure and guide zinc deposition in the more uniform manner.

To evaluate the performance of NSCDs as electrolyte additives, 2 M $ZnSO_4$ aqueous solutions with different concentrations of NSCDs were used as the electrolytes for Zn||Zn symmetric cells, and named as ZS-NSCDx (x = 0.1, 0.2, 0.4, 1 mg mL^{-1}) (Fig. S2). As shown in Fig. 3a and S3, at different current densities from 1 mA cm^{-2} to 10 mA cm^{-2}, ZS-NSCD0.2 exhibit the lowest polarization voltage, while ZS-NSCD0.1 had the higher polarization voltage. In the constant current cycle tests at 1 mA cm^{-2} and 0.5 mAh cm^{-2} (Fig. 3b, S4), all samples show good cycle stability, demonstrating the excellent performance of NSCDs as the electrolyte additive. ZS-NSCD0.1 and ZS-NSCD1 had relatively short lifetimes of 1865 h and 2083 h, respectively, while ZS-NSCD0.2 completed more than 4000 h of cycling with a stationary voltage curve, which is significantly better than those data in recent reports

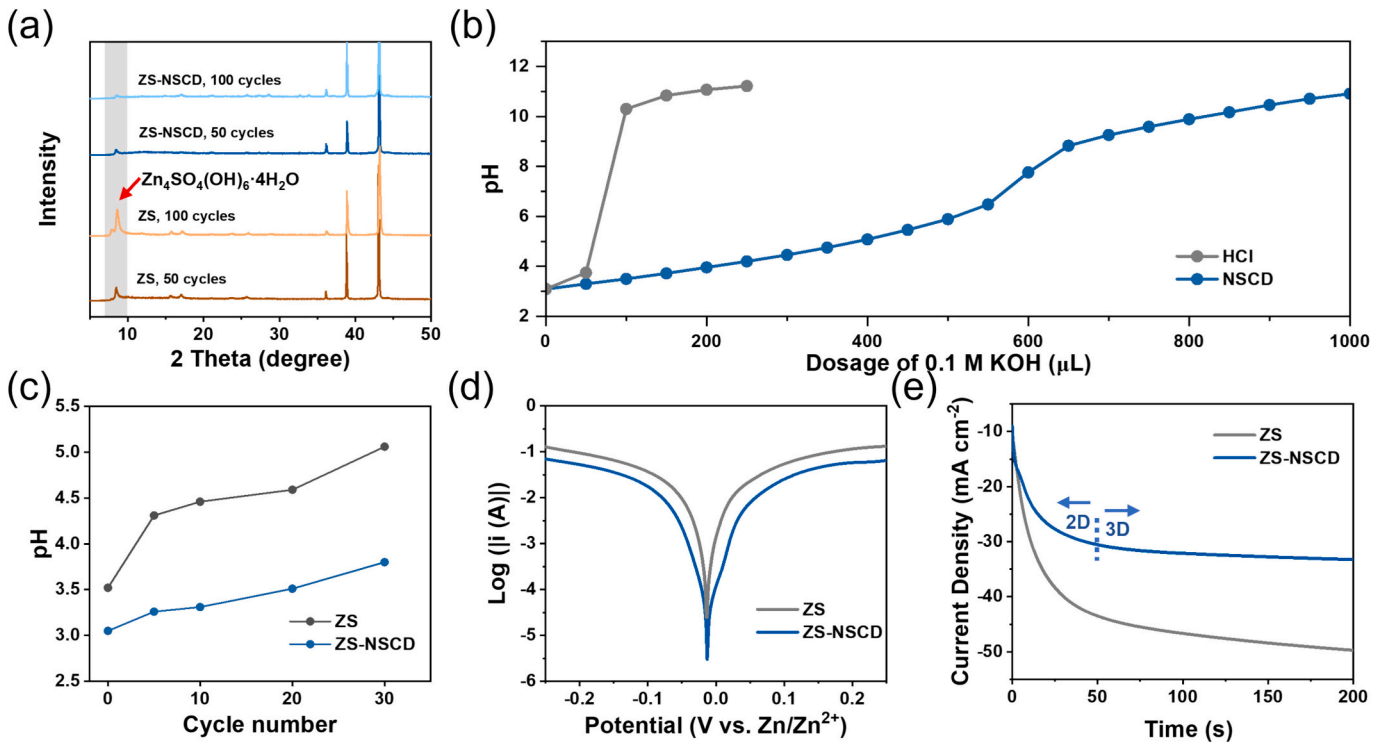

Fig. 4. (a) Comparison of XRD patterns of zinc anodes after 50 and 100 cycles at 1 mA cm^{-2} and 0.5 mAh cm^{-2}. (b) Titration 10 mL of NSCD and HCl solution with 0.1 mol NaOH as the titrant. (c) The pH of the electrolyte after 0, 5, 10, 20, 30 cycles. (d)Tafel plots representing corrosion behaviors. (e) CA curves indicating Zn^{2+} diffusion process of Zn electrode in ZS and ZS-NSCD electrolytes, respectively.

(Fig. 3c, Table S1). The shorter lifetime of the high-concentration group is due to the increased viscosity of the electrolyte and the decrease of ion conductivity (Fig. S5), Furthermore, the aggregation of NSCDs at high concentrations is also a contributing factor to performance degradation. Although NSCDs exhibit good solubility in deionized water, their solubility is significantly impaired in the high ionic strength environment of the 2 M $ZnSO_4$ electrolyte. At elevated concentrations, NSCDs cannot dissolve effectively and tend to aggregate. These aggregated NSCD particles can lead to the formation of an uneven interface on the electrode surfaces, thereby adversely affecting battery performance. In contrast, the control cell using 2 M $ZnSO_4$ electrolyte can only maintain 60 cycles of cycling before a rapidly short-circuiting. Based on the above tests, the optimal NSCDs concentration was determined to be 0.2 mg mL^{-1}, and the subsequent tests and cell assemblies will use the ZS-NSCD0.2 sample. For the sake of brevity, ZS-NSCD0.2 is abbreviated as ZS-NSCD in the following text.

Subsequently, the stability of ZS-NSCD assembled cells were tested at different current densities respectively, and ZS-NSCD maintained stable cycling and a small polarization voltage from 1 mA cm^{-2} to 10 mA cm^{-2} (Fig. S6). In the subsequent deep discharge test, the ZS-NSCD group symmetric cell remained stable for more than 200 h at 10 mA cm^{-2} and 10 mAh cm^{-2} (Fig. S7). The shortened lifespan under higher depth of discharge (DOD) is primarily due to the excessive amount of zinc deposition/stripping under those conditions, which exceeds the capability of NSCDs to regulate uniform deposition. This leads to a significant reduction in electrode surface flatness. The SEM images (Fig. S8) shows that the surface of the failed electrode exhibits numerous pits and grooves, and substantial dendrite growth piercing the separator leads to short circuits. These various tests demonstrate the stable cycling ability of symmetric cells after using NSCD as an electrolyte additive. In addition, the surface conditions of the electrodes during the symmetric cell cycling process were characterized. Fig. 3d shows the SEM and EDS images of the zinc plate after 50 cycles of symmetric cell cycling in ZS-NSCD, with a smooth and flat surface and only a few oxygen-containing by-products. In contrast, the zinc plate after cycling in ZS have lots of plate-like species on the surface, and the EDS results confirm that the surface oxygen content is very high, indicating the generation of by-products. The surface morphology of the zinc plate during the deposition process was observed using *in-situ* optical microscopy (Fig. 3e, f). During the one-hour deposition process, large dendrites appear on the surface of zinc plate in ZS due to uneven deposition, while the zinc plate in ZS-NSCD maintain a flat surface morphology owing to the positive effects of NSCDs.

In the XRD patterns of the zinc plates after cycling in different electrolytes (Fig. 4a), the samples from the ZS-NSCD electrolyte show the typical zinc diffraction with almost no impurities, while the samples from the ZS electrolyte exhibit the peaks of $Zn_4SO_4(OH)_6{\cdot}4H_2O$ that is the common by-product in literature. These by-products are derived from the side reactions between Zn and the active H_2O in the Helmholtz layer, especially under the increased pH values. The pH enhancement is a common phenomenon when the HER and the H^+ insertion take place in AZIBs. Hence, maintaining a relatively stable pH value of the electrolyte is very important to the stability of AZIBs. To investigate the mechanism of NSCDs in suppressing side reactions, their pH-stabilizing capability are examined in aqueous solutions (Fig. 4b). When 0.1 M KOH solution (pH = 12.82) is gradually added into 10 mL of NSCDs solution with HCl (initial pH = 3.09), the pH value of the mixture keeps below 6 even after the added KOH solution reaches 500 μL, demonstrating excellent pH buffer effects of NSCDs. In contrast, a control HCl aqueous solution (pH = 3.10) shows quite different behavior, that only 100 μL of KOH addition can increases the pH value from 3.10 to 10.30. Such a pH buffering performance of NSCDs are owing to the abundant surface carboxyl and amine groups, for amine groups consume excess H^+ under low pH conditions, while carboxyl groups release H^+ to neutralize OH^- under high pH conditions. During the cycling of AZIBs, the electrode surface is prone to the following side reactions:

$$2H_2O + 2e^- \rightarrow 2OH^- + H_2$$

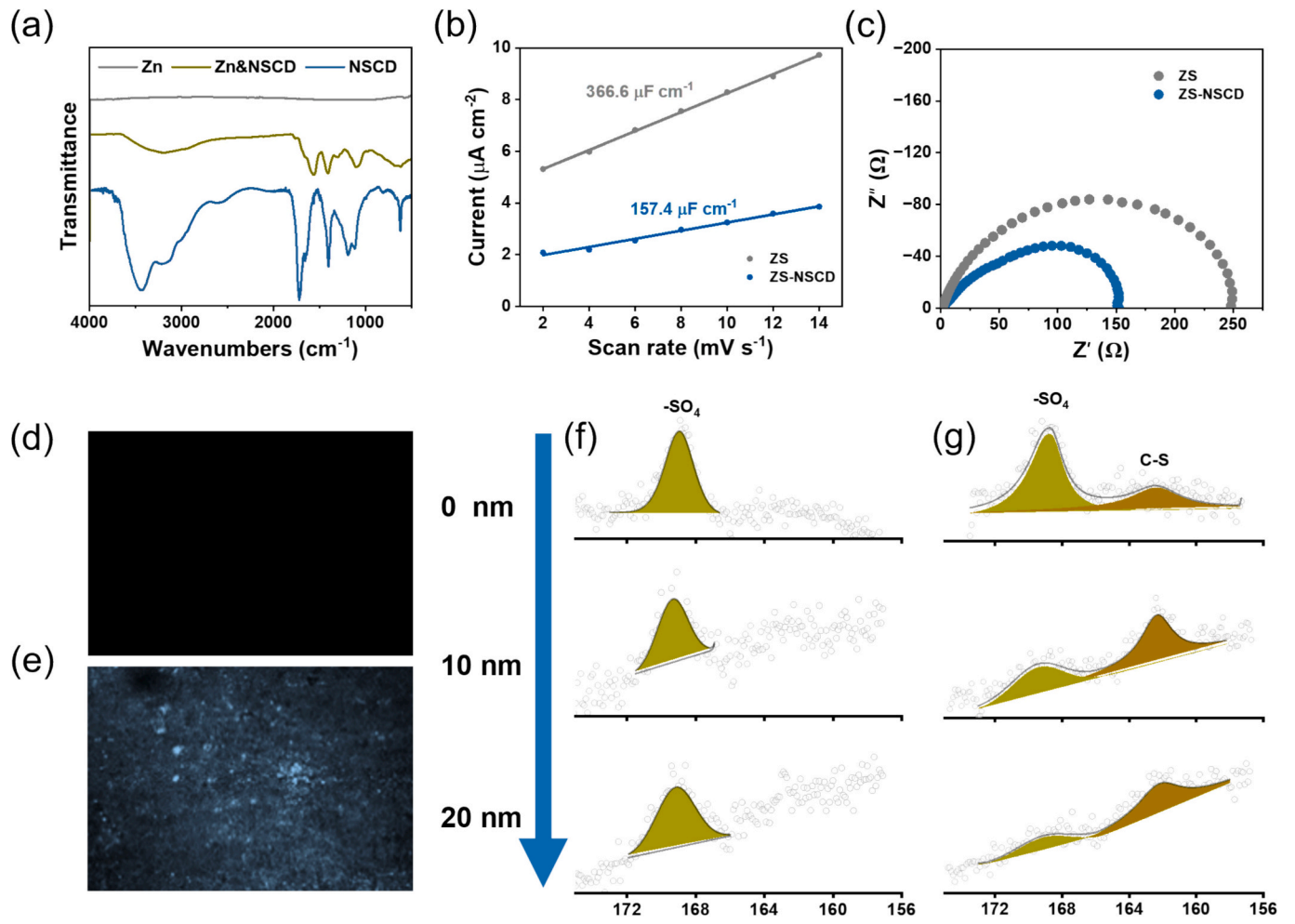

Fig. 5. (a) ATR-FTIR spectra of bare Zn, NSCD and Zn&NSCD; (b) EDL capacitance at zinc electrode in ZS and ZS-NSCD; (c) EIS profiles of Zn||Zn cells with ZS and ZS-NSCD electrolyte before cycling; Confocal luminescence image of Zn plate in Zn||Zn cells with (d) ZS and (e) ZS-NSCD after 30 cycles; The XPS depth spectra for S 2p of Zn anode tested in (f) ZS and (g)ZS-NSCD electrolyte for 30 cycles.

$$3Zn^{2+} + 6OH^{-} + ZnSO_4 + xH_2O \rightarrow Zn_4SO_4(OH)_6 \cdot xH_2O$$

The HER-induced pH elevation facilitates the formation of electrochemically inert byproducts. However, the NSCDs additives are able to maintain a lower pH environment effectively near the electrode, thereby significantly suppressing byproduct generation [46]. In fact, due to their strong adsorption on the zinc electrode surface, NSCDs will have the higher local concentration at the electrode/electrolyte interface than that in the bulk electrolyte. Therefore, only a small addition of NSCDs can contribute a great buffering capacity and stabilize the pH values on the electrode/electrolyte interfaces.

The pH evolution of the electrolyte in Zn||Zn symmetric cells is monitored during plating/stripping cycles at 1 mA cm^{-2} and 0.5 mAh cm^{-2} to evaluate the pH-buffering effect of NSCDs under operational conditions (Fig. 4c). The initial pH value of 2 M $ZnSO_4$ electrolyte increases from 3.52 to 5.06 after 30 cycles due to the severe HER. Notably, the interfacial pH at the electrode surface is typically much higher than the bulk electrolyte value, which would accelerate side reactions and byproduct formation, ultimately compromising the electrode stability [47]. In contrast, the 2 M $ZnSO_4$ electrolyte containing 0.2 mg mL^{-1} of NSCDs shows different behavior. Although its initial pH is slightly lower (3.05, attributed to H^+ release from NSCDs), it demonstrates significantly improved pH stability during cycles, maintaining a relatively low pH of 3.80 even after 30 cycles. These results confirm that NSCDs effectively function as pH buffers in 2 M $ZnSO_4$ electrolyte, maintaining a relatively acidic environment that suppresses excessive byproduct formation and preserves electrode integrity during prolonged cycling.

The Zn||Zn symmetric cell using the basic 2 M $ZnSO_4$ electrolyte exhibited a large nucleation overpotential (Fig. S9), which caused Zn^{2+} to deposit at a few easily nucleated sites, leading to Zn dendrites. After adding NSCDs, the graphitic N and sulfamine groups in NSCDs will coordinate with Zn to increase the nucleation sites effectively [48], and reduce the nucleation overpotential to 52.39 mV. A lower nucleation overpotential means a lower nucleation barrier, which is conducive to the uniform Zn deposition [49,50]. Tafel curves of the symmetric cells are shown in Fig. 4d, and the cell using ZS-NSCD exhibits the lower corrosion current than the control (0.15 *vs* 2.15 mA cm^{-2}), indicating that the addition of CDs enhances the corrosion resistance of the electrode. The linear sweep voltammetry (LSV) curve in Fig. S10 shows that the ZS-NSCD cell has a larger overpotential (38 mV), which means that the hydrogen evolution reaction during cycling is better suppressed. In addition, at the other end of the curve, the evolution of O_2 is also inhibited. This protective effect arises from the NSCDs adsorption layer on the electrode interface which significantly reduces the content of reactive water molecules in the Helmholtz layer, thereby enhancing the electrode's resistance to the aqueous corrosion. The above experimental results demonstrate that the NSCDs protective layers on the zinc electrodes are able to enhance the electrode's electrochemical stability effectively.

Chronoamperometry (CA) measurements are employed to investigate Zn^{2+} diffusion behaviors during zinc deposition, for the current transients can reflect the morphological evolution of the electrode. In

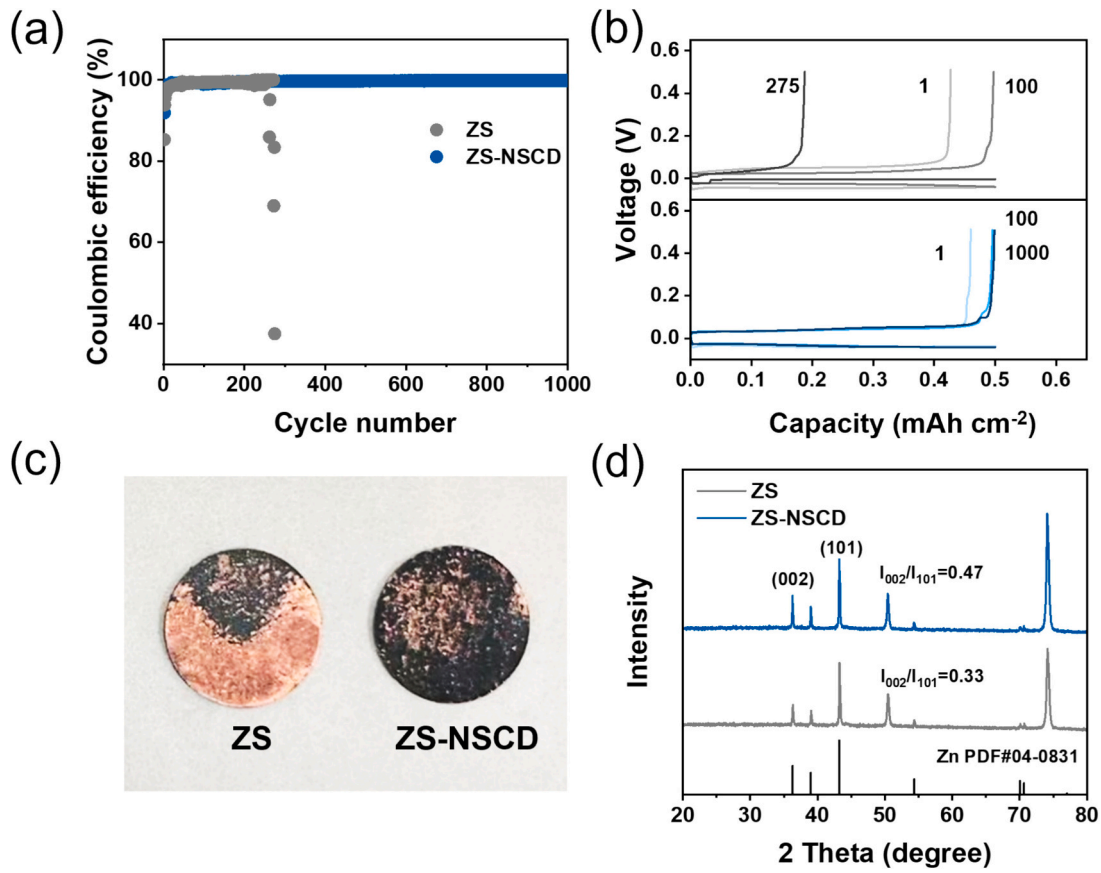

Fig. 6. (a) CE of Zn||Cu half cells with ZS and ZS-NSCD electrolyte at 1 mA cm^{-2} and 0.5 mAh cm^{-2}. (b) the corresponding voltage profiles at different cycles. (c) digital images and (d) XRD patterns of Cu plate in Zn||Cu half cells after deposition of 5mAh cm^{-2} zinc.

Fig. 4e, the ZS sample exhibits a continuous current increase over 200 s, indicating the prolonged 2D diffusion of Zn^{2+} ions as they search for low-surface-energy sites, leading to the localized deposition and the dendrite formation. In contrast, the ZS-NSCD sample changes from the initial 2D diffusion (~50 s) to a stable 3D diffusion, evidenced by the steady current profile corresponding to the uniform Zn deposition. These results demonstrate that the *in situ*-formed CDs interlayer can confine Zn^{2+} 2D diffusion, where the strong coordination interactions between Zn^{2+} and oxygen-containing functional groups of CDs restrict the deposition to the proximal sites of the initial adsorption, and in the meantime, promote the formation of numerous small nucleation sites. This mechanism significantly enhances the homogeneity of zinc deposition, as evidenced by the observations under an optical microscopy [51,52].

The adsorption effects of NSCDs on the Zn metal surface are evaluated by various tests. Firstly, the zinc plate is soaked in an aqueous solution containing 0.2 mg mL^{-1} of NSCDs for 24 h, and then analyzed by ATR-FTIR. As shown in the Fig. 5a, the bare zinc shows no obvious characteristic peaks, but after NSCDs soaking, multiple peaks corresponding to NSCDs appear. It is noticed that the peak positions of C═C (1650 cm^{-1}) and O═S═O (1100 cm^{-1}) exhibit some redshift, which can be attributed to the strong interactions between these groups and Zn surface [53]. Secondly, the electrochemical double layer capacitance (EDLC) of the Zn||Zn symmetric cells using ZS and ZS-NSCD was measured respectively (Fig. S11). In Fig. 5b, the EDLC using ZS is 366.6 μF cm^{-1}, while that using ZS-NSCD is only 157.4 μF cm^{-1}. This indicates that the strong adsorption of NSCDs on the zinc surface drives away the original H_2O molecules in the inner Helmholtz planes, resulting in a decrease in EDLC [54–56]. Thirdly, in the electrochemical impedance spectroscopy (EIS) test (Fig. 5 c), compared to the control group, the ZS-NSCD cell exhibits a significantly reduced charge transfer resistance (R_{ct}), indicating that the *in-situ* formed interfacial layer structure by CDs facilitates the desolvation and ion transport processes. Further tests are conducted to examine the impedance changes of symmetric cells during long-term cycling (Fig. S12). Due to those uncontrolled side reactions within the cell, a large amount of non-conductive byproducts accumulated on the electrode surface, causing the impedance of the ZS symmetric cell to increase rapidly during cycles. In contrast, the ZS-NSCD symmetric cell maintain the lower impedance after 100 cycles. The impedance decrease at the 5th cycle compared to the initial state is usually attributed to the further formation of the interfacial layer. This phenomenon demonstrates that the ZS-NSCD electrolyte can effectively mitigate side reactions within the cell, suppress the formation of passivation layers on the electrode surface, thereby ensuring rapid charge transfer processes and reducing the charge transfer impedance of the cell. Finally, the confocal microscopy images (Fig. 5 d and e) also confirm the existence of the interface layer. After 50 cycles working, the electrode slices are washed by ethanol and deionized water, and then the dried samples are observed by a confocal microscope. It is clear the Zn plate soaked in the ZS-NSCD electrolyte exhibits the blue fluorescence of CDs, while the control shows no fluorescence signal.

The XPS with Ar^+ sputtering depth profile is used to analyze the composition distribution of the interface layer on the Zn plate (Fig. S13). The C 1 s spectra reveal that the electrode surface consists of $ZnCO_3$ (289 eV) and characteristic carbonaceous components C-H/C-C (284.8 eV). With increasing depth, the $ZnCO_3$ signal weakens while the C═O (287 eV) signal gradually intensifies (Fig. S14). Furthermore, the S 2p spectra confirm the depth-dependent compositional distribution within the interfacial layer (Fig. 5 f and g). A distinct SO_4^{2-} peak (168.9 eV) is observed at the surface [57], originating from both the $ZnSO_4$ electrolyte and accumulated $Zn_4SO_4(OH)_6$ byproducts. This signal significantly diminishes in the inner interfacial layer, where the organic C—S (162.4

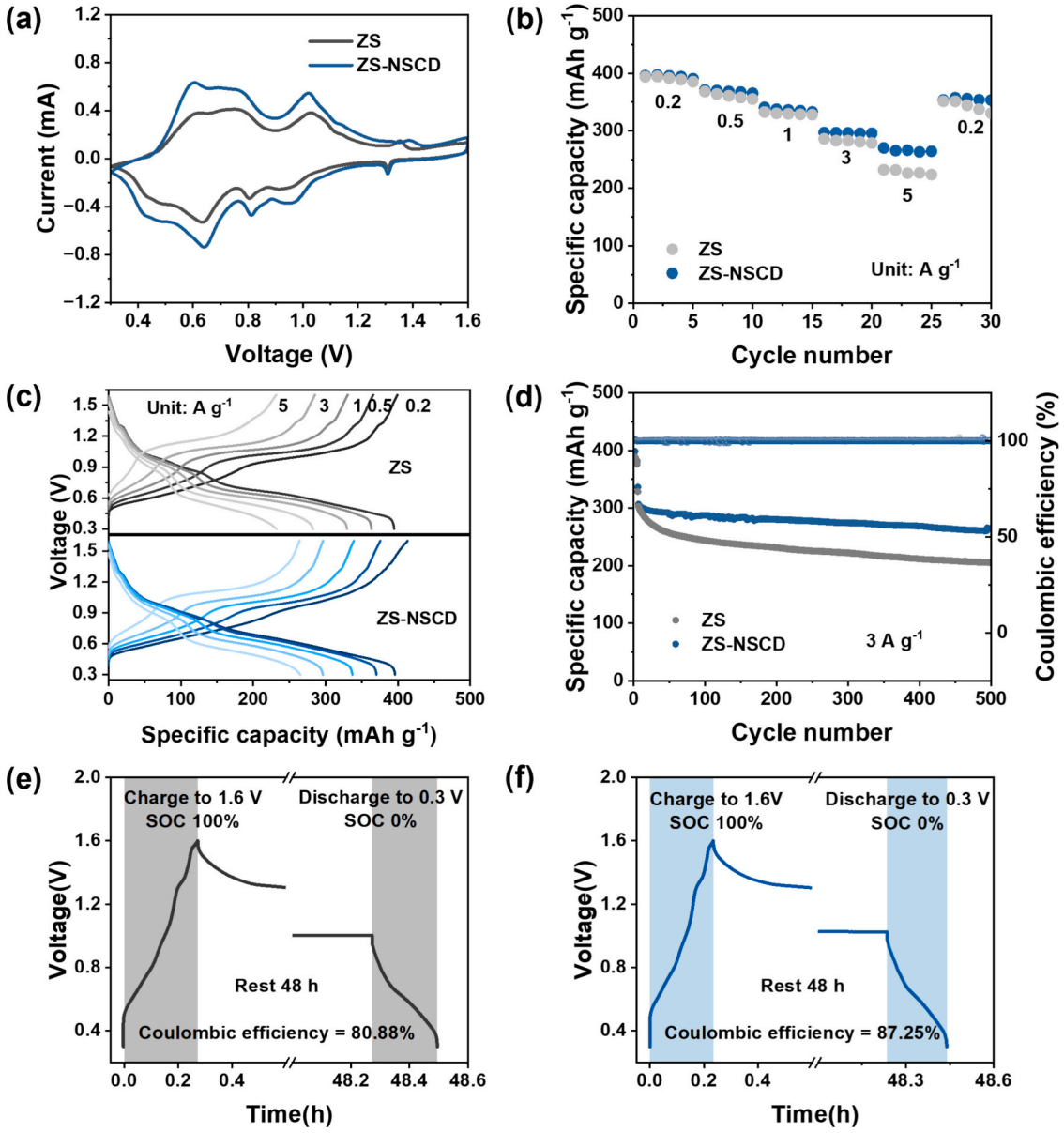

Fig. 7. Electrochemical performance of Zn||NVO cells using ZS and ZS-NSCD electrolytes, respectively. (a) CV curves at a scan rate of 0.5 mV s^{-1}; (b) rate performance of Zn||NVO cells; (c) charge-discharge profiles under different current density conditions; (d) cycling performance and CE of Zn||NVO cells with mass loading 1.19 mg cm^{-2}; self-discharge analyses of Zn||NVO cells using (e) ZS and (f) ZS-NSCD electrolytes.

eV) component from carbon dots becomes dominant [58]. In contrast, zinc electrodes cycled in ZS electrolyte show markedly different behavior, with no significant spectral changes observed as a function of sputtering depth. These results demonstrate that ZS-CD forms a unique interfacial layer on the electrode surface: an outer region composed of $ZnSO_4$, $ZnCO_3$, and byproducts, and an inner organic-inorganic composite layer primarily consisting of NSCDs. This structure effectively enhances the electrode's corrosion resistance and stability.

After disassembling a Zn||ZS-NSCD0.2||Zn symmetric cell cycled for 50 cycles, the electrode was taken out, washed with deionized water thoroughly, and then reassembled into a new symmetric cell using 2 M $ZnSO_4$ electrolyte. The cycling performance under the same conditions (1 mA cm^{-2}, 0.5 mAh cm^{-2}) is shown in Fig. S15. The symmetric cell achieved stable cycling for over 700 h, representing a significant increase compared to the control cell's lifespan of less than 100 h. This experiment demonstrates that after initial cycles NSCDs have formed interfacial protective layers on the Zn electrode surfaces.

To further evaluate the ability of NSCDs to achieve uniform zinc flux and inhibit Zn dendrite growth, the reversibility of Zn deposition and stripping was measured using a Zn||Cu half cells assembly. As shown in Fig. 6a and b, in the first few cycles, due to the process of reshaping the zinc coordination, the coulombic efficiency (CE) is low. In the subsequent 200 cycles, both groups of cells maintain stable CE. However, due to the dendrite growth and the by-product formation, the ZS half-cell exhibits severe fluctuations and soon short-circuits. In contrast, the ZS-NSCD half-cell, which presents a clear contrast, could cycle steadily for over 1000 times and maintain a high CE. After depositing Zn at 5 mAh cm^{-2} on the copper foil, the half-cells are disassembled to observe the morphologies of the electrode foils (Fig. 6c). In the ZS group the copper foil is covered by zinc on a few positions, while in the ZS-NSCD group the copper foil is uniformly covered by zinc on almost all the surface. This strongly demonstrates the ability of NSCD additive to promote uniform deposition of Zn^{2+}. The SEM images of the sample of the ZS group (Fig. S16) show that a large amount of loose and disorder zinc accumulated on the copper foil surface, accompanied by many flaky by-products. In contrast, the zinc deposition in the ZS-NSCD group is

more uniform and compact, only with fewer by-products. The XRD patterns in Fig. 4i shows that the zinc deposited in the ZS-NSCD group has a relatively high I_{002}/I_{101} value. Those previous reports point out that the (101) planes of zinc are aligned with the substrate at large degrees, which are prone to the growth of dendrites. However, the (002) planes of zinc are aligned with the substrate at $0 \sim 30^{o}$, resulting in the denser and more uniform zinc deposition to suppress corrosion and dendrites [59]. The above results confirm the ability of NSCDs to achieve uniform zinc flux and inhibit dendrite growth reasonably.

ZS-NSCD and ZS are assembled into Zn||$NH_4V_4O_{10}$ (NVO) full cells to study their performance respectively, in which NVO is synthesized according to the previous literature (Fig. S17, S18) [60]. The initial cyclic voltammetry (CV) tests (Fig. 7a) reveal that both cells exhibit similar electrochemical behavior, confirming that the introduction of NSCDs does not alter the redox reactions [61]. As shown in Fig. 7 b and c, the full cell employing the ZS-NSCD electrolyte demonstrates superior rate capability across various current densities (0.1, 0.2, 1, 3, and 5 A g^{-1}). Notably, even at high current densities, the NSCDs additive facilitates rapid redox kinetics and stable interfacial charge transfer [62]. A comparison of the cycling performance at 3 A g^{-1} (Fig. 7d) shows that the cell with ZS-NSCD electrolyte delivers an initial capacity of 306.9 mAh g^{-1} after activation and retains 260.5 mAh g^{-1} after 500 charge/discharge cycles, significantly outperforming the cell with ZS electrolyte (84.9 % *vs.* 69.3 % of the capacity retention). Furthermore, Fig. 7 e and f present the self-discharge behavior of the two cells after a 48-h rest period following charging, as evaluated by CE. The ZS-NSCD cell maintains a CE of 87.25 % after resting, whereas the ZS cell only achieves 80.88 %. These results demonstrate that the NSCDs additive effectively suppresses side reactions and dendrite formation during cycles, thereby enhancing the overall electrochemical performance of the full cells.

3. Conclusion

This study suggests a novel strategy of constructing an interfacial protective layer *in situ* on Zn anode by adding multifunctional NSCDs of only 0.2 mg mL^{-1} into the common $ZnSO_4$ electrolyte. Various experimental characterizations and theoretical calculations demonstrate that such an inorganic-organic hybrid layer can protect Zn electrodes and stabilize the AZIBs through three aspects. Firstly, NSCDs replace some active water molecules in the Helmholtz layer to reduce the electrode corrosion significantly. Secondly, NSCDs facilitate the desolvation process of the hydrated Zn^{2+} ions, and serve as additional nucleation sites to guide uniform zinc deposition. Finally, NSCDs act as pH buffers to effectively mitigate the interfacial pH increase caused by HER, consequently reducing the formation of byproducts. As a result, the dendrite growth on the zinc electrode is effectively inhibited, and the cycling life of the AZIBs is significantly prolonged. In comparison with those reports about the electrolyte additives for AZIBs, our NSCDs modified batteries exhibit remarkable performance. The assembled Zn||Zn symmetric cell achieves stable cycling for over 4000 h at 1 mA cm^{-2} and 0.5 mAh cm^{-2}, and the Zn||NVO full cell demonstrates a high specific capacity with a long-time cycling stability. Our present work provides new insights on the design and application of CDs as electrolyte additives for AZIBs from the perspective of interfacial engineering.

CRediT authorship contribution statement

Qian-Li Ma: Writing – original draft, Visualization, Validation, Software, Investigation, Formal analysis, Data curation. **Xi-Rong Zhang:** Visualization, Formal analysis, Data curation. **Bao-Juan Wang:** Validation, Investigation, Formal analysis. **Hao-Wen Sun:** Visualization, Data curation. **Huan-Ming Xiong:** Writing – review & editing, Supervision, Resources, Project administration, Methodology, Investigation, Funding acquisition, Conceptualization.

Declaration of competing interest

The authors declare that they have no known competing financial interests or personal relationships that could have appeared to influence the work reported in this paper.

Acknowledgements

This work was financially supported by the National Natural Science Foundation of China (U24A20565, 22575057) and the Science and Technology Commission of Shanghai Municipality (25ZR1401024).

Appendix A. Supplementary data

Supplementary data to this article can be found online at https://doi.org/10.1016/j.cej.2026.172570.

Data availability

Data will be made available on request.

References

[1] J. Cao, D. Zhang, X. Zhang, Z. Zeng, J. Qin, Y. Huang, Strategies of regulating Zn^{2+} solvation structures for dendrite-free and side reaction-suppressed zinc-ion batteries, Energy Environ. Sci. 15 (2) (2022) 499–528, https://doi.org/10.1039/D1EE03377H.
[2] J. Hao, X. Li, S. Zhang, F. Yang, X. Zeng, S. Zhang, G. Bo, C. Wang, Z. Guo, Designing dendrite-free zinc anodes for advanced aqueous zinc batteries, Adv. Funct. Mater. 30 (30) (2020) 2001263, https://doi.org/10.1002/adfm.202001263.
[3] T.C. Li, D. Fang, J. Zhang, M.E. Pam, Z.Y. Leong, J. Yu, X.L. Li, D. Yan, H.Y. Yang, Recent progress in aqueous zinc-ion batteries: a deep insight into zinc metal anodes, J. Mater. Chem. A 9 (10) (2021) 6013–6028, https://doi.org/10.1039/D0TA09111A.
[4] P. Ruan, S. Liang, B. Lu, H.J. Fan, J. Zhou, Design strategies for high-energy-density aqueous zinc batteries, Angew. Chem. Int. Ed. 61 (17) (2022) e202200598, https://doi.org/10.1002/anie.202200598.
[5] J. Liu, W. Zhou, R. Zhao, Z. Yang, W. Li, D. Chao, S.-Z. Qiao, D. Zhao, Sulfur-based aqueous batteries: electrochemistry and strategies, J. Am. Chem. Soc. 143 (38) (2021) 15475–15489, https://doi.org/10.1021/jacs.1c06923.
[6] T.-B. Song, Q.-L. Ma, X.-R. Zhang, J.-W. Ni, T.-L. He, H.-M. Xiong, Zn anode surface engineering for stable zinc-ion batteries: carbon dots incorporated mesoporous TiO_2 as a coating layer, Chem. Eng. J. 471 (2023) 144735, https://doi.org/10.1016/j.cej.2023.144735.
[7] P. Sun, L. Ma, W. Zhou, M. Qiu, Z. Wang, D. Chao, W. Mai, Simultaneous regulation on solvation shell and electrode interface for dendrite-free Zn ion batteries achieved by a low-cost glucose additive, Angew. Chem. Int. Ed. 60 (33) (2021) 18247–18255, https://doi.org/10.1002/anie.202105756.
[8] Y.-S. Li, L.-S. Geng, B.-M. Zhang, Z.-H. Wei, H. Fan, J.-H. Li, W.-C. Feng, L. Zhou, Concentrated perchlorate-based electrolyte facilitates Zn anode-compatible in situ solid electrolyte interphase, Rare Metals 44 (2) (2025) 950–960, https://doi.org/10.1007/s12598-024-02972-7.
[9] J.-H. Lee, R. Kim, S. Kim, J. Heo, H. Kwon, J.H. Yang, H.-T. Kim, Dendrite-free Zn electrodeposition triggered by interatomic orbital hybridization of Zn and single vacancy carbon defects for aqueous Zn-based flow batteries, Energy Environ. Sci. 13 (9) (2020) 2839–2848, https://doi.org/10.1039/D0EE00723D.
[10] D. Yuan, J. Zhao, H. Ren, Y. Chen, R. Chua, E.T.J. Jie, Y. Cai, E. Edison, W. Manalastas Jr., M.W. Wong, M. Srinivasan, Anion texturing towards dendrite-free Zn anode for aqueous rechargeable batteries, Angew. Chem. Int. Ed. 60 (13) (2021) 7213–7219, https://doi.org/10.1002/anie.202015488.
[11] L. Liu, X. Wang, Z. Hu, X. Wang, Q. Zheng, C. Han, J. Xu, X. Xu, H.-K. Liu, S.-X. Dou, W. Li, Electric double layer regulator design through a functional group assembly strategy towards long-lasting zinc metal batteries, Angew. Chem. Int. Ed. 63 (30) (2024) e202405209, https://doi.org/10.1002/anie.202405209.
[12] K. Feng, B. Chen, B. Xi, C. Tian, B. Sang, S. Meng, Y. He, T. Gao, X. An, G. Zhou, S. Xiong, X. Wang, Antioxidant interfaces enabled by self-deoxidizing and delf-dehydrogenating redox couple for reversible zinc metal batteries, Adv. Energy Mater. 14 (29) (2024) 2401053, https://doi.org/10.1002/aenm.202401053.
[13] F. Wan, L.L. Zhang, X. Dai, X.Y. Wang, Z.Q. Niu, J. Chen, Aqueous rechargeable zinc/sodium vanadate batteries with enhanced performance from simultaneous insertion of dual carriers, Nat. Commun. 9 (2018), https://doi.org/10.1038/s41467-018-04060-8.
[14] Y.M. Zhang, H.N. Li, S.Z. Huang, S. Fan, L.N. Sun, B.B. Tian, F.M. Chen, Y. Wang, Y. M. Shi, H.Y. Yang, Rechargeable aqueous zinc-ion batteries in $MgSO_4/ZnSO_4$ hybrid electrolytes, Nano Micro Lett. 12 (1) (2020), https://doi.org/10.1007/s40820-020-0385-7.
[15] G. Chang, S. Liu, Y. Fu, X. Hao, W. Jin, X. Ji, J. Hu, Inhibition role of trace metal ion additives on zinc dendrites during plating and striping processes, advanced materials, Interfaces 6 (23) (2019), https://doi.org/10.1002/admi.201901358.

[16] L. Ma, S. Chen, H. Li, Z. Ruan, Z. Tang, Z. Liu, Z. Wang, Y. Huang, Z. Pei, J. A. Zapien, C. Zhi, Initiating a mild aqueous electrolyte Co_3O_4/Zn battery with 2.2 V-high voltage and 5000-cycle lifespan by a co(iii) rich-electrode, Energy Environ. Sci. 11 (9) (2018) 2521–2530, https://doi.org/10.1039/C8EE01415A.
[17] S. Hosseini, S.J. Han, A. Arponwichanop, T. Yonezawa, S. Kheawhom, Ethanol as an electrolyte additive for alkaline zinc-air flow batteries, Sci. Rep. 8 (2018), https://doi.org/10.1038/s41598-018-29630-0.
[18] K.E.K. Sun, T.K.A. Hoang, T.N.L. Doan, Y. Yu, X. Zhu, Y. Tian, P. Chen, Suppression of dendrite formation and corrosion on zinc anode of secondary aqueous batteries, ACS Appl. Mater. Interfaces 9 (11) (2017) 9681–9687, https://doi.org/10.1021/acsami.6b16560.
[19] C.W. Lee, K. Sathiyanarayanan, S.W. Eom, H.S. Kim, M.S. Yun, Novel electrochemical behavior of zinc anodes in zinc/air batteries in the presence of additives, J. Power Sources 159 (2) (2006) 1474–1477, https://doi.org/10.1016/j.jpowsour.2005.11.074.
[20] Z. Hou, M. Dong, Y. Xiong, X. Zhang, H. Ao, M. Liu, Y. Zhu, Y. Qian, A high-energy and long-life aqueous Zn/birnessite battery via deversible water and Zn^{2+} coinsertion, Small 16 (26) (2020), https://doi.org/10.1002/smll.202001228.
[21] R. Cheng, Y. Xiang, R. Guo, L. Li, G. Zou, C. Fu, H. Hou, X. Ji, Structure and interface modification of carbon dots for electrochemical energy application, Small 17 (40) (2021) 2102091, https://doi.org/10.1002/smll.202102091.
[22] J.-S. Wei, C. Ding, P. Zhang, H. Ding, X.-Q. Niu, Y.-Y. Ma, C. Li, Y.-G. Wang, H.-M. Xiong, Robust negative electrode materials derived from carbon dots and porous hydrogels for high-performance hybrid supercapacitors, Adv. Mater. 31 (5) (2019) 1806197, https://doi.org/10.1002/adma.201806197.
[23] J.-W. Ni, X.-R. Zhang, T.-B. Song, Z.-H. Huang, Q.-L. Ma, T.-L. He, H.-M. Xiong, Robust polymer electrolytes with fast ion-transport nanochannels constructed by carbon dots for long lifespan Li metal batteries, Chem. Eng. J. 500 (2024) 157379, https://doi.org/10.1016/j.cej.2024.157379.
[24] H. Liu, L. Xu, F. Zhu, D. Luo, Y. Zhang, W. Deng, G. Zou, H. Hou, X. Ji, Unveiling the effect law of carbon dots with polyfunctional groups on interface structure and ion migration in polymer electrolytes for solid lithium battery, Nano Energy 126 (2024) 109623, https://doi.org/10.1016/j.nanoen.2024.109623.
[25] T.-B. Song, Q.-L. Ma, B.-J. Wang, X.-R. Zhang, Y.-G. Wang, H.-M. Xiong, High-capacity and long-life cathode constructed solely by carbon dots for aqueous zinc-ion batteries, Angew. Chem. Int. Ed. 64 (34) (2025) e202503655, https://doi.org/10.1002/anie.202503655.
[26] S. Li, L. Li, H. Tu, H. Zhang, D.S. Silvester, C.E. Banks, G. Zou, H. Hou, X. Ji, The development of carbon dots: from the perspective of materials chemistry, Mater. Today 51 (2021) 188–207, https://doi.org/10.1016/j.mattod.2021.07.028.
[27] C. Xia, J. Zhong, X. Han, S. Zhu, Y. Li, H. Liu, B. Yang, The formation mechanism of carbonized polymer dots: crosslinking-induced nucleation and carbonization, Angew. Chem. Int. Ed. 63 (44) (2024) e202410519, https://doi.org/10.1002/anie.202410519.
[28] B. Wang, G.I.N. Waterhouse, B. Yang, S. Lu, Advances in shell and core engineering of carbonized polymer dots for enhanced applications, Acc. Chem. Res. 57 (19) (2024) 2928–2939, https://doi.org/10.1021/acs.accounts.4c00516.
[29] H. Zhang, R. Guo, S. Li, C. Liu, H. Li, G. Zou, J. Hu, H. Hou, X. Ji, Graphene quantum dots enable dendrite-free zinc ion battery, Nano Energy 92 (2022) 106752, https://doi.org/10.1016/j.nanoen.2021.106752.
[30] W. Zhang, M. Dong, K. Jiang, D. Yang, X. Tan, S. Zhai, R. Feng, N. Chen, G. King, H. Zhang, H. Zeng, H. Li, M. Antonietti, Z. Li, Self-repairing interphase reconstructed in each cycle for highly reversible aqueous zinc batteries, Nat. Commun. 13 (1) (2022) 5348, https://doi.org/10.1038/s41467-022-32955-0.
[31] W.J. Lee, J. Lim, S.O. Kim, Nitrogen dopants in carbon nanomaterials: defects or a new opportunity? Small Methods 1 (1–2) (2017) 1600014 https://doi.org/10.1002/smtd.201600014.
[32] T.B. Song, Z.H. Huang, X.R. Zhang, J.W. Ni, H.M. Xiong, Nitrogen-doped and sulfonated carbon dots as a multifunctional additive to realize highly reversible aqueous zinc-ion batteries, Small 19 (31) (2023) e2205558, https://doi.org/10.1002/smll.202205558.
[33] Q. Ma, T. Song, T. He, X. Zhang, H. Xiong, Sulfur-doped carbon dots: a novel bifunctional electrolyte additive for high-performance aqueous zinc-ion batteries, Acta Phys. -Chim. Sin. 41 (9) (2025) 100106, https://doi.org/10.1016/j.actphy.2025.100106.
[34] G.-D. Yang, J.-H. Wang, Z. Wang, Q.-M. Zhang, S.-M. Zhou, X.-Y. Huang, B. Yang, H.-Z. Sun, D.S. Seferos, Carbonized polymer dots with intelligent recognition and dynamic protection for highly stable Zn-ion batteries, J. Colloid Interface Sci. 700 (2025) 138499, https://doi.org/10.1016/j.jcis.2025.138499.
[35] S.J. Mohammed, K.M. Omer, F.E. Hawaiz, Deep insights to explain the mechanism of carbon dot formation at various reaction times using the hydrothermal technique: FT-IR, (13)C-NMR, (1)H-NMR, and UV-visible spectroscopic approaches, RSC Adv. 13 (21) (2023) 14340–14349, https://doi.org/10.1039/d3ra01646c.
[36] R.V. Nair, P.R. Chandran, A.P. Mohamed, S. Pillai, Sulphur-doped graphene quantum dot based fluorescent turn-on aptasensor for selective and ultrasensitive detection of omethoate, Anal. Chim. Acta 1181 (2021) 338893, https://doi.org/10.1016/j.aca.2021.338893.
[37] M. Moniruzzaman, J. Kim, Shape-engineered carbon quantum dots embedded on CdS-nanorods for enhanced visible light harvesting towards photocatalytic application, Appl. Surf. Sci. 552 (2021) 149372, https://doi.org/10.1016/j.apsusc.2021.149372.
[38] Y. Zhu, J. Li, X. Yun, G. Zhao, P. Ge, G. Zou, Y. Liu, H. Hou, X. Ji, Graphitic carbon quantum dots modified nickel cobalt sulfide as cathode materials for alkaline aqueous batteries, Nano Micro Lett. 12 (1) (2020) 16, https://doi.org/10.1007/s40820-019-0355-0.
[39] S. Qin, X. Yu, L. Xu, Amplified fluorescence detection and adsorption of Au^{3+} by the fluorescent melamine formaldehyde microspheres incorporated with N and S co-doped carbon dots, J. Hazard. Mater. 405 (2021) 123978, https://doi.org/10.1016/j.jhazmat.2020.123978.
[40] M. Pajewska-Szmyt, B. Buszewski, R. Gadzała-Kopciuch, Sulphur and nitrogen doped carbon dots synthesis by microwave assisted method as quantitative analytical nano-tool for mercury ion sensing, Mater. Chem. Phys. 242 (2020) 122484, https://doi.org/10.1016/j.matchemphys.2019.122484.
[41] H. Zhang, Z. Luo, W. Deng, J. Hu, G. Zou, H. Hou, X. Ji, Interfacial reconstruction via electronegative sulfonated carbon dots in hybrid electrolyte for ultra-durable zinc battery, Chem. Eng. J. 461 (2023) 142105, https://doi.org/10.1016/j.cej.2023.142105.
[42] D. Hong, Y. Choi, J. Ryu, J. Mun, W. Choi, M. Park, Y. Lee, N.-S. Choi, G. Lee, B.-S. Kim, S. Park, Homogeneous Li deposition through the control of carbon dot-assisted Li-dendrite morphology for high-performance Li-metal batteries, J. Mater. Chem. A 7 (35) (2019) 20325–20334, https://doi.org/10.1039/C9TA06260B.
[43] J. Wolska, K. Stawicka, J. Walkowiak-Kulikowska, Sulfonic-acid-functionalized polymers based on fluorinated methylstyrenes and styrene as promising heterogeneous catalysts for esterification, Mater. Chem. Phys. 273 (2021) 125132, https://doi.org/10.1016/j.matchemphys.2021.125132.
[44] S. Daniuk, T. Jarlborg, G. Kontrym-Sznajd, J. Majsnerowski, H. Stachowiak, Electronic structure of Mg, Zn and cd, J. Phys. Condens. Matter 1 (44) (1989) 8397, https://doi.org/10.1088/0953-8984/1/44/011.
[45] H. Yang, K. Zhu, W. Xie, W. Yang, Enhancing zinc anode reversibility through dynamic interface engineering with monolayer hydrophobic carbon dots, ACS Nano 19 (1) (2025) 1433–1446, https://doi.org/10.1021/acsnano.4c14244.
[46] H. Li, L. Yang, S. Zhou, J. Li, Y. Chen, X. Meng, D. Xu, C. Han, H. Duan, A. Pan, A self-regulated interface enabled by multi-functional pH buffer for reversible Zn electrochemistry, Adv. Funct. Mater. 34 (19) (2024) 2313859, https://doi.org/10.1002/adfm.202313859.
[47] K. Ouyang, S. Chen, W. Ling, M. Cui, Q. Ma, K. Zhang, P. Zhang, Y. Huang, Synergistic modulation of in-situ hybrid interface construction and pH buffering enabled ultra-stable zinc anode at high current density and areal capacity, Angew. Chem. Int. Ed. Eng. 62 (45) (2023) e202311988, https://doi.org/10.1002/anie.202311988.
[48] W. Zhou, M. Chen, Q. Tian, J. Chen, X. Xu, C.-P. Wong, Cotton-derived cellulose film as a dendrite-inhibiting separator to stabilize the zinc metal anode of aqueous zinc ion batteries, Energy Storage Mater. 44 (2022) 57–65, https://doi.org/10.1016/j.ensm.2021.10.002.
[49] F. Xie, H. Li, X. Wang, X. Zhi, D. Chao, K. Davey, S.-Z. Qiao, Mechanism for zincophilic sites on zinc-metal anode hosts in aqueous batteries, Adv. Energy Mater. 11 (9) (2021) 2003419, https://doi.org/10.1002/aenm.202003419.
[50] L. Geng, J. Meng, X. Wang, W. Wu, K. Han, M. Huang, C. Han, L. Wu, J. Li, L. Zhou, L. Mai, Organic-solvent-free primary solvation shell for low-temperature aqueous zinc batteries, Chem 11 (2) (2025) 102302, https://doi.org/10.1016/j.chempr.2024.09.001.
[51] M. Han, J. Huang, X. Xie, T.C. Li, J. Huang, S. Liang, J. Zhou, H.J. Fan, Hydrated eutectic electrolyte with ligand-oriented solvation shell to boost the stability of zinc battery, Adv. Funct. Mater. 32 (25) (2022) 2110957, https://doi.org/10.1002/adfm.202110957.
[52] A. Bayaguud, X. Luo, Y. Fu, C. Zhu, Cationic surfactant-type electrolyte additive enables three-dimensional dendrite-free zinc anode for stable zinc-ion batteries, ACS Energy Lett. 5 (9) (2020) 3012–3020, https://doi.org/10.1021/acsenergylett.0c01792.
[53] B. Wang, R. Zheng, W. Yang, X. Han, C. Hou, Q. Zhang, Y. Li, K. Li, H. Wang, Synergistic solvation and interface regulations of eco-friendly silk peptide additive enabling stable aqueous zinc-ion batteries, Adv. Funct. Mater. 32 (23) (2022) 2112693, https://doi.org/10.1002/adfm.202112693.
[54] G. Guo, C. Ji, J. Lin, T. Wu, Y. Luo, C. Sun, M. Li, H. Mi, L. Sun, H.J. Seifert, Interfacial domino effect triggered by β-alanine cations realized highly reversible zinc-metal anodes, Angew. Chem. Int. Ed. 63 (33) (2024) e202407417, https://doi.org/10.1002/anie.202407417.
[55] Z.Y. Shen, J.L. Mao, G.P. Yu, W.D. Zhang, S.L. Mao, W. Zhong, H. Cheng, J.Z. Guo, J.H. Zhang, Y.Y. Lu, Electrocrystallization regulation enabled stacked hexagonal platelet growth toward highly reversible zinc anodes, Angew. Chem. Int. Ed. 62 (11) (2023), https://doi.org/10.1002/anie.202218452.
[56] C. Yan, H.-R. Li, X. Chen, X.-Q. Zhang, X.-B. Cheng, R. Xu, J.-Q. Huang, Q. Zhang, Regulating the inner helmholtz plane for stable solid electrolyte interphase on lithium metal anodes, J. Am. Chem. Soc. 141 (23) (2019) 9422–9429, https://doi.org/10.1021/jacs.9b05029.
[57] X.-R. Yu, F. Liu, Z.-Y. Wang, Y. Chen, Auger parameters for sulfur-containing compounds using a mixed aluminum-silver excitation source, J. Electron Spectrosc. Relat. Phenom. 50 (2) (1990) 159–166, https://doi.org/10.1016/0368-2048(90)87059-W.
[58] S. Pignataro, L. Lunazzi, C.A. Boicelli, R. Di Marino, A. Ricci, A. Mangini, R. Danieli, Charge density distribution in organo-metal sulfides by means of ^{13}C NMR and S_{2p32} ESCA chemical shifts, Tetrahedron Lett. 13 (52) (1972) 5341–5344, https://doi.org/10.1016/S0040-4039(01)85245-X.
[59] D.J. Mackinnon, J.M. Brannen, P.L. Fenn, Characterization of impurity effects in zinc electrowinning from industrial acid sulphate electrolyte, J. Appl. Electrochem. 17 (6) (1987) 1129–1143, https://doi.org/10.1007/BF01023596.
[60] D. Xu, Z. Wang, C. Liu, H. Li, F. Ouyang, B. Chen, W. Li, X. Ren, L. Bai, Z. Chang, A. Pan, H. Zhou, Water catchers within sub-nano channels promote step-by-step

zinc-ion dehydration enable highly efficient aqueous zinc-metal batteries, Adv. Mater. 36 (26) (2024) e2403765, https://doi.org/10.1002/adma.202403765.

[61] T. Zhu, B. Mai, P. Hu, Z. Liu, C. Cai, X. Wang, L. Zhou, Ammonium ion and structural water co-assisted Zn^{2+} intercalation/De-intercalation in $NH_4V_4O_{10}$•0.28H_2O†, Chin. J. Chem 39 (7) (2021) 1885–1890, https://doi.org/10.1002/cjoc.202100004.

[62] Z. Wei, X. Wang, T. Zhu, P. Hu, L. Mai, L. Zhou, Mitigating the dissolution of V_2O_5 in aqueous $ZnSO_4$ electrolyte through Ti-doping for zinc storage, Chin. Chem. Lett. 35 (1) (2024) 108421, https://doi.org/10.1016/j.cclet.2023.108421.